Chemical Science

ROYAL SOCIETY OF CHEMISTRY

EDGE ARTICLE

View Article Online
View Journal | View Issue

Cite this: *Chem. Sci.*, 2025, **16**, 3928

All publication charges for this article have been paid for by the Royal Society of Chemistry

Periodic law-guided design of highly stable O3-type layered oxide cathodes for practical sodium-ion batteries†

Yuan-Bo Wu,[ab] Hai-Yan Hu,*[abc] Jia-Yang Li,[c] Hang-Hang Dong,[b] Yan-Fang Zhu,*[ab] Shuang-Qiang Chen,[ab] Na-Na Wang,[c] Jia-Zhao Wang [b] and Yao Xiao *[abd]

O3-type $NaNi_{0.5}Mn_{0.5}O_2$ cathode material exhibits significant potential for sodium-ion batteries (SIBs) owing to its high theoretical capacity and ample sodium reservoir. Nonetheless, its practical implementation encounters considerable obstacles, such as impaired structural integrity, sensitivity to moisture, inadequate high-temperature stability, and being unstable under high-voltage conditions. This study investigates the co-substitution of Cu, Mg, and Ti, guided by principles of the periodic law, to enhance the material's stability under varying conditions. The substituent elements were selected based on their atomic properties and introduced into specific sites within the structure: Cu and Mg were substituted at Ni sites, while Ti replaced Mn sites. These modifications strengthened the crystal lattice, mitigating phase transitions, and improved electrochemical performance. The O3-type $NaNi_{0.4}Cu_{0.05}Mg_{0.05}Mn_{0.3}Ti_{0.2}O_2$ material exhibited remarkable moisture stability, maintaining 85% of its capacity after 1000 cycles at 5C in 2.0–4.0 V. It also exhibited reversible phase transitions at voltages up to 4.3 V, with no oxygen release observed even when charged to 4.5 V. Furthermore, it exhibited remarkable high-temperature stability in half-cell testing and excellent cycling performance in full-cell evaluations. These results are very helpful for designing high-performance SIB cathodes that can withstand a variety of operating circumstances and ensuring structural stability.

Received 10th December 2024
Accepted 14th January 2025

DOI: 10.1039/d4sc08351b

rsc.li/chemical-science

Introduction

Sodium-ion batteries (SIBs) have emerged as a plausible and affordable alternative to lithium-ion batteries.[1–3] Their appeal lies in the plentiful and evenly distributed nature of sodium resources relative to lithium, which bodes well for large-scale, low-cost energy storage.[4,5] In addition, SIBs have greater safety thanks to the more stable electrochemical behaviours of sodium, reducing risks such as thermal runaway.[6] It is for these reasons that SIBs are particularly fascinating in areas where reliable and secure energy is required, emphasizing both cost-effectiveness and material abundance.[7] Nonetheless, amidst these promising aspects, the development of efficient SIBs in turn depends largely on the breakthroughs in high-performance cathode materials. This is the key to determining energy density, life span, and safety like yet a viable, less expensive and lower-risk candidate for today's batteries.[8,9]

Currently, O3-type $NaNi_{0.5}Mn_{0.5}O_2$ (NaNM) is acknowledged as a promising candidate for SIB cathodes due to its impressive capacity and cycle stability, along with its relatively simple synthesis process.[10] These attributes make it a strong contender for Na^+ storage applications.[11] However, NaNM suffers from a number of limitations that place obstacles in the way of practical application. These include the following: (a) structural instability: NaNM undergoes multiple phase transitions $O3_{hex} - O3'_{mon} - P3_{hex} - P'3_{mon} - P3'_{hex} - O3'_{hex}$, which cause severe distortion of the crystal structure during Na^+ extraction and insertion.[12] This leads to problems such as grain cracking, voltage hysteresis and reduction in capacity durability.[13] Repetition of these charge–discharge cycles aggravates these problems, and high-voltage cycling further accelerates the inevitable phase changes and lattice distortions that damage the long-term stability of the material.[14,15] (b) Moisture sensitivity: NaNM is highly sensitive to moisture, which results in surface degradation.[16] The reaction of moisture with NaNM leads to production of unwanted by-products, such as NaOH and Na_2CO_3, on the particle surfaces.[17] These increase interfacial resistance, even further lowering the electrical performance of

[a]College of Chemistry and Materials Engineering, Wenzhou University, Wenzhou, 325035, P. R. China. E-mail: hyh927@uowmail.edu.au; yanfangzhu@wzu.edu.cn; xiaoyao@wzu.edu.cn

[b]Wenzhou Key Laboratory of Sodium-Ion Batteries, Wenzhou University Technology Innovation Institute for Carbon Neutralization, Wenzhou, 325035, P. R. China

[c]Institute for Superconducting and Electronic Materials, Australian Institute for Innovative Materials, University of Wollongong Innovation Campus, North Wollongong, NSW 2522, Australia

[d]Key Laboratory of Advanced Energy Materials Chemistry (Ministry of Education), Nankai University, Tianjin, 300071, P. R. China

† Electronic supplementary information (ESI) available. See DOI: https://doi.org/10.1039/d4sc08351b

the material, reducing the chances that it will work well in real-world settings.[18] (c) Poor high-temperature performance: NaNM's performance deteriorates at elevated temperatures due to its sensitivity to thermal fluctuations, which affect the stability of the crystal lattice. Prolonged exposure at high temperatures speeds up phase transitions and introduces distortions to the lattice, which in turn affect the material's structural integrity.[19] After that, the material's durability and performance at high temperature fall off as well. While NaNM holds significant potential as a SIB cathode material, addressing these challenges through further material optimization is crucial for its practical application in commercial energy storage solutions.[20]

In response to the shortcomings of NaNM, several strategies have been suggested, including those involving surface coatings, ion substitution, and modifications to the structure of crystals.[21–23] Among these strategies, ion substitution has shown promising potential for improving material stability. Therefore, this work examines the strategic co-substitution within the O3-type NaNM structure of Cu, Mg, and Ti guided by principles periodic law in order to get materials that are more stable. Co-substitution in practice reinforces the material's structure and helps to suppress phase transitions, particularly under high-charge conditions. The choice of Cu, Mg, and Ti as substitution elements was based on a detailed analysis of their atomic orbital configurations, electron arrangement, ionic radii and charge state.[24] These properties were carefully considered to optimize their effects on the host structure and to determine the appropriate substitution sites within the material. Optimization of these properties allows the co-substitution strategy to address both the structural and electrochemical challenges implicit in NaNM. Specifically, substituting Cu and Mg for Ni enhances the material by suppressing irreversible phase transitions and improving structural stability. Substituting Mn with Ti will enhance the stability by increasing high-voltage stability and stabilizing lattice oxygen. These synergistic effects together give the material moisture stability, high voltage stability, structural stability, and high-temperature stability. The O3-$NaNi_{0.4}Cu_{0.05}Mg_{0.05}Mn_{0.3}Ti_{0.2}O_2$ (NaNCMMT) material demonstrates excellent moisture stability, achieving 85% capacity retention after 1000 cycles at 5C in 2–4 V, with completely reversible phase transitions during cycling. Even under extended voltage conditions up to 4.3 V, the phase transitions remain reversible. Notably, there is no oxygen release observed even when it is charged to 4.5 V. The cathode also exhibits strong high-temperature stability, demonstrating favorable capacity retention. In full-cell evaluations, it shows outstanding cycling stability and reversibility, even without pre-sodiation. This study provides scientific insights into tuning the structure and electrochemical balance of sodium-layered oxides to support the systematic design of sodium-ion cathodes with enhanced performance under diverse practical conditions.

Results and discussion

To enhance the electrochemical performance of O3-type layered NaNM cathodes, the strategic selection of substituent elements is essential.[25,26] The principle that structure dictates properties guided the choice of Cu, Mg, and Ti, leveraging their periodic characteristics.[27,28] The elemental properties, such as electronic configurations, atomic radii, and predominant oxidation states, display periodic trends due to the structured variation in electron arrangements as nuclear charge increases.[29–31] This periodicity stems from the fundamental arrangement of electrons outside the atomic nucleus, influencing how atoms and their resulting ions interact with surrounding environments.[32,33] As shown in Fig. 1a, Cu and Mg were selected for substitutions at the Ni sites based on similarities in electron configuration and ionic radius. Both Cu^{2+} and Mg^{2+} share an ionic radius of approximately 72 pm and exhibit a consistent +2 charge state, which helps maintain structural stability within the NaNM framework. Additionally, Ti was chosen to occupy Mn sites due

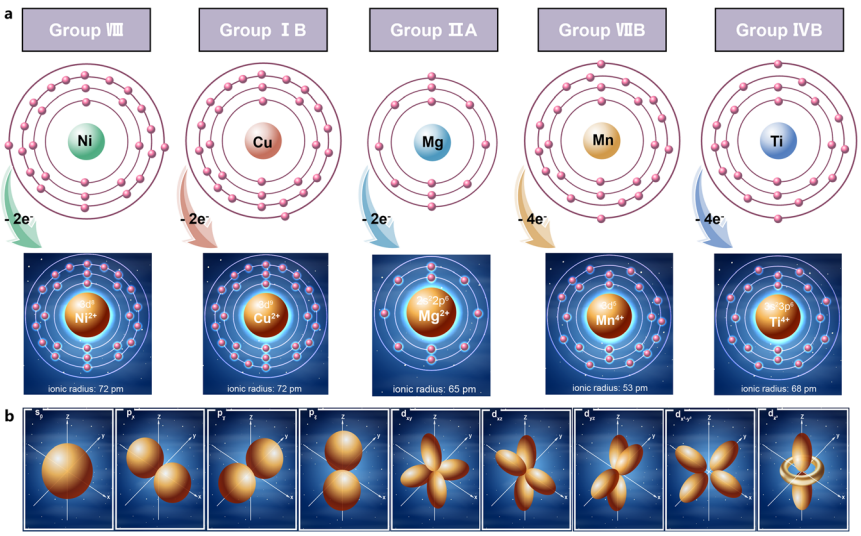

Fig. 1 (a) The atomic orbital configurations and outer electron arrangements of Ni, Cu, Mg, Mn, Ti. (b) Schematic of the distribution of s, p, d atomic orbital types.

to comparable ionic properties, supporting uniform distribution without substantial lattice distortion.[34] The similar electron cloud densities and shapes of these substituent elements—such as spherically symmetric s-orbitals or p-orbitals—were also considered (Fig. 1b). These orbitals affect how the electrons contribute to structural stability and ionic conductivity.[35] From a microscale perspective, electrons move rapidly within confined atomic spaces (diameters around 10^{-10} m) with unpredictable trajectories, characterized as electron clouds. This understanding emphasizes the significance of electron probability density in assessing substituent elements' behavior. For instance, spherical s-orbitals distribute electron density evenly, while p- and d-orbitals create specific, directional bonding effects. The nuanced orbital interactions of Cu, Mg, and Ti ensure tailored modifications to NaNM's electronic structure and ion diffusion pathways. This methodical selection and placement of substituent elements enable substantial advancements in material performance, aligning with the desired electrochemical enhancements.

The crystal structure of NaNCMMT was analyzed using powder X-ray diffraction (XRD) with Rietveld refinement, as illustrated in Fig. 2a and b.[36] The XRD results confirmed that the material exhibits a hexagonal O3 phase with an $R\bar{3}m$ space group, indicating the successful synthesis of the O3-type layered structure.[37] The detailed structural parameters, such as lattice constants ($a = 2.96761$ Å, $b = 2.96761$ Å, $c = 16.13333$ Å), and the low values of R_p and R_{wp}, signify a strong correlation between the experimental and calculated patterns, validating the accuracy of the crystallographic data.[38] The morphology of NaNCMMT was further examined using scanning electron microscopy (SEM) and transmission electron microscopy (TEM). The SEM image (Fig. S1, ESI†) revealed that NaNCMMT exhibits chunk-like morphology. High-resolution TEM (HR-TEM) images (Fig. 2c; and S2, ESI†) provided detailed information about the crystalline facets, showing interplanar lattice spacings of 0.52 nm, which correspond to the (003) planes of the O3 phase.[39] The HR-TEM analysis corroborates the XRD findings, confirming the well-defined O3 structure of NaNCMMT. Besides, inductively coupled plasma mass spectrometry (ICP-MS) analysis of the sample, as shown in Table S1, ESI† confirms the successful synthesis of the NaNCMMT cathode material. The wettability of NaNCMMT was assessed by analyzing the three-phase interaction among gas, solid, and liquid. As shown in Fig. S3a, ESI†, the interfacial tensions between solid–vapor (γ_{SV}), solid–liquid (γ_{SL}), and liquid–vapor (γ_{LV}) were considered, and Young's equation, $\gamma_{LV}\cos(\mathcal{C}) = \gamma_{SV} - \gamma_{SL}$, was applied to determine the contact angle.[40] The measured wetting angle for NaNCMMT was 94.27°, indicating hydrophobic behavior, while NaNM exhibited a wetting angle of 67.79°, reflecting hydrophilic properties (Fig. 2d, e; and Tables S2, S3, ESI†).[41] The hydrophobic nature of NaNCMMT suggests that its surface repels water, thereby reducing interaction with moisture and preventing penetration. The material's stability was further confirmed through soaking experiments. The consistent XRD patterns before and after soaking (Fig. 2f) demonstrate that NaNCMMT maintains its structural integrity, with robust metal–oxygen bonds that resist hydrolysis and moisture-induced degradation. Furthermore, the infrared spectroscopy (IR) analysis of the material post-soaking only exhibited weak CO_3^{2-} peaks, indicating minimal surface reaction and strong chemical stability in aqueous conditions (Fig. S3b, ESI†).[42,43] These findings suggest that the material's

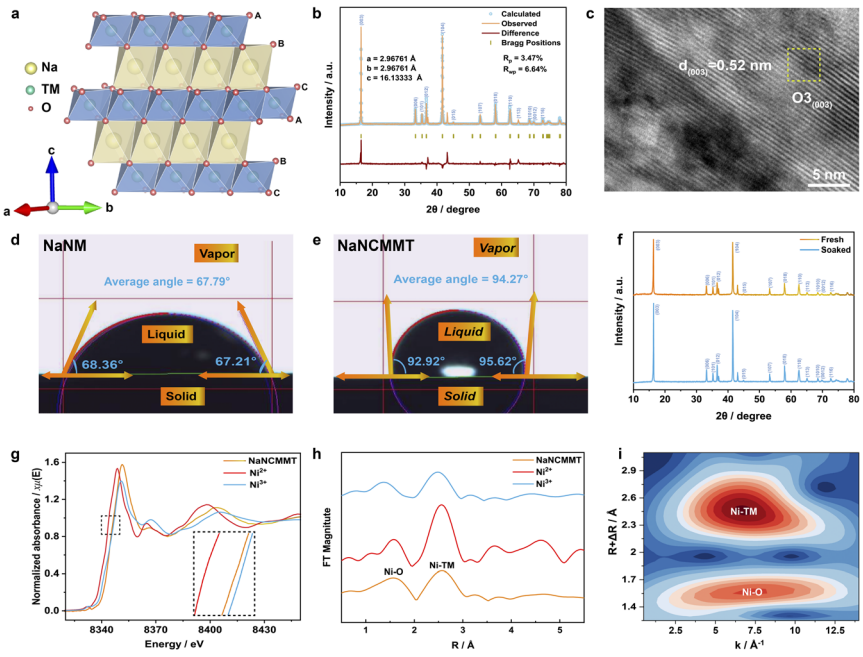

Fig. 2 Structure of NaNCMMT cathode material. (a) Structural illustration of O3-type ($R\bar{3}m$) structure. (b) XRD pattern and rietveld refinement. (c) HR-TEM image. (d) Wetting angle of NaNM. (e) Wetting angle of NaNCMMT. (f) Comparison of XRD patterns of NaNCMMT before and after soaking in water. (g) XANES spectra at Ni K-edge. (h) Fourier transformation of EXAFS at Ni K-edge. (i) WT-EXAFS spectra at Ni K-edge.

intrinsic structural stability, combined with its hydrophobic surface properties, effectively prevents oxidation and ensures durability in moist environments. To explore the influence of Cu, Mg, and Ti co-substitution on the valence states of elements within NaNCMMT, X-ray photoelectron spectroscopy (XPS) was employed, as presented in Fig. S4, ESI†. The weak satellite peaks observed in Fig. S4c, ESI† suggest the possible presence of both divalent and trivalent nickel.[44] This conclusion is consistent with the X-ray absorption near-edge structure (XANES) spectra at the Ni K-edge (Fig. 2g), which provide complementary evidence for the divalent and trivalent states of Ni after co-substitution.[45] Further structural insights were gained from Fourier transform of extended X-ray absorption fine structure (FT-EXAFS) and wavelet transform EXAFS (WT-EXAFS). These analyses clearly visualized the Ni–O and Ni-transition metal (TM) bonds, providing a deeper understanding of the local coordination environment and the effects of co-substitution on the Ni sites (Fig. 2h and i).

The Na^+ storage performance of the NaNCMMT cathode was systematically assessed using coin-type half-cells with a Na metal anode.[46,47] At a voltage window of 2.0–4.0 V, the NaNCMMT cathode demonstrated a reversible capacity of 123.43 mA h g^{-1} at 0.1C (12 mA g^{-1}, Fig. 3a). Furthermore, it exhibited excellent rate performance, retaining 68.3% of its initial capacity at 5C compared to 0.1C (Fig. 3b and c). The cathode's impressive cycling stability was evident with 85% capacity retention after 1000 cycles at 5C (Fig. 3d), and consistent retention rates of 93.4% and 98.1% after 300 cycles at 1C and 100 cycles at 2C, respectively (Fig. S5, ESI†). Cyclic voltammetry (CV) at 0.1 mV s^{-1} revealed peaks that aligned well with the galvanostatic charge–discharge profiles, suggesting the absence of complex phase transitions and highlighting stable

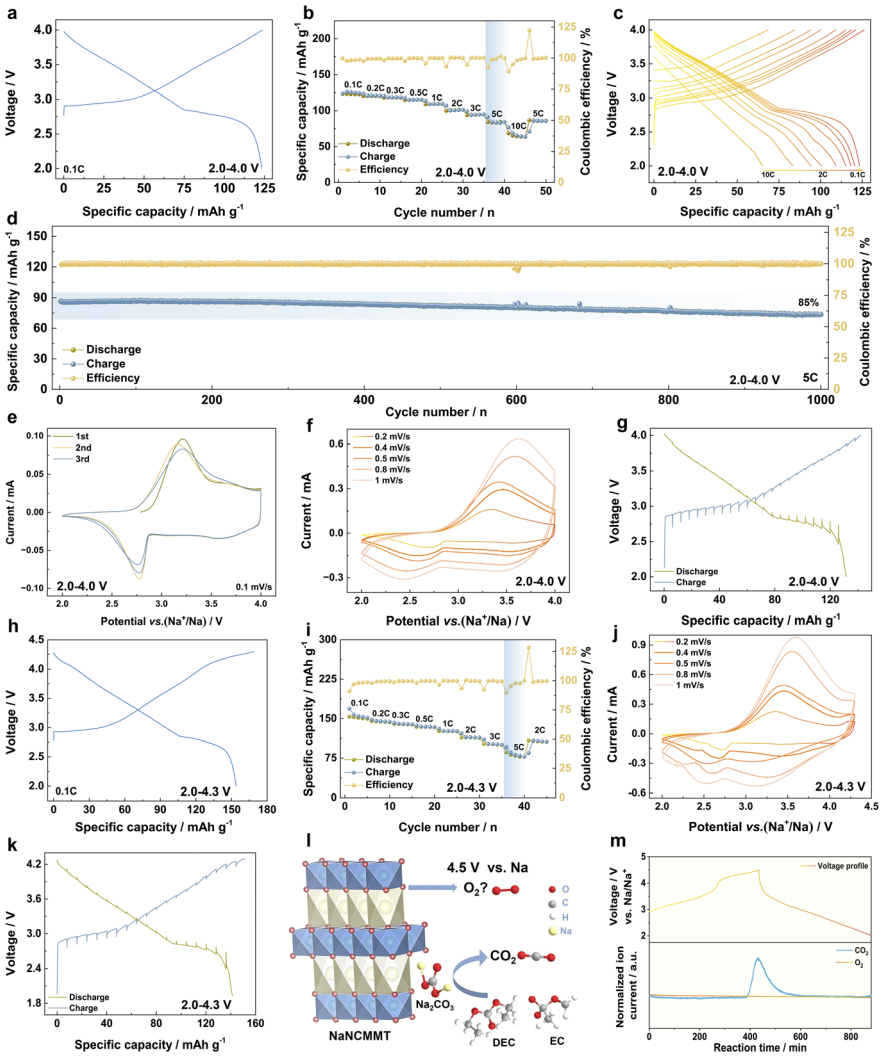

Fig. 3 Electrochemical performance of NaNCMMT cathode. (a) Charge–discharge curves at 0.1C in 2.0–4.0 V. (b and c) Rate performance at various rates and the corresponding galvanostatic charge/discharge curves in 2.0–4.0 V. (d) Cycle performance during 1000 cycles at 5C in 2.0–4.0 V. (e) CV curves at 0.1 mV s^{-1} in 2.0–4.0 V. (f) CV curves at different scan rates in 2.0–4.0 V. (g) GITT curves in 2.0–4.0 V. (h) Charge–discharge curves at 0.1C in 2.0–4.3 V. (i) Rate performance at various rates in 2.0–4.3 V. (j) CV curves at different scan rates in 2.0–4.3 V. (k) GITT curves in 2.0–4.3 V. (l) Illustration of O_2 and CO_2 outgassing from NaNCMMT upon charging at 4.5 V. (m) O_2 and CO_2 gas evolution from NaNCMMT electrode during the first cycle in 2.0–4.5 V.

electrochemical characteristics (Fig. 3e).[48,49] The study of Na^+ transport kinetics using CV scans at different rates highlighted a primarily capacitive sodium storage mechanism, as indicated by a calculated *b*-value of 0.85 (Fig. 3f; S6a and b, ESI†). The galvanostatic intermittent titration technique (GITT) analysis supported this finding, with minimal ohmic (13.7 mV) and voltage polarization (77.9 mV) observed, signifying efficient ionic transport (Fig. 3g; S6c and d, ESI†).[50] To further understand the material's performance across a wider voltage range, tests were extended to 2.0–4.3 V.[51] In this range, the NaNCMMT cathode achieved a higher reversible capacity of 153.9 mA h g^{-1} at 0.1C (16 mA g^{-1}, Fig. 3h). Even under high-rate conditions, the capacity retention was steady, maintaining 66.3% at 5C (Fig. 3i; S7a, ESI†) and 64.4% after 100 cycles at 2C (Fig. S7b, ESI†). Consistent with previous observations, CV curves at 0.1 mV s^{-1} aligned with the charge–discharge profiles (Fig. S7c, ESI†), and the Na^+ kinetics analysis yielded a *b*-value of 0.93, further confirming the dominant capacitive mechanism (Fig. 3j; S8a and b, ESI†). GITT analysis showed low ohmic (26.2 mV) and voltage polarization (85.8 mV, Fig. 3k; S8c and d, ESI†), emphasizing stable electrochemical performance. The extended voltage window testing provided crucial insights into the high-voltage performance of the layered oxide cathode.[52] As illustrated in the schematic (Fig. 3l), charging up to 4.5 V induces oxygen release from the structure due to intensified overlap and electronic interactions between the O 2p orbitals and TM 3d orbitals at elevated oxidation states. This interaction redistributes electron density away from the oxygen atoms, weakening the TM–O bonds, destabilizing the lattice, and ultimately facilitating lattice oxygen release.[53] This reflects the intrinsic instability of layered oxides at elevated potentials, where extensive Na extraction and overlapping electronic states promote oxygen oxidation.[54] Additionally, the observed CO_2 release predominantly originated from electrolyte decomposition rather than from the cathode material itself.[55] Differential electrochemical mass spectrometry (DEMS) characterized the gas evolution, showing negligible O_2 outgassing but significant CO_2 emission (Fig. 3m). The electrochemical performance of the NaNCMMT cathode is shown in Fig. S9 (ESI†). Even when charged to 4.5 V, the cathode retains 62.4% of its capacity at 2C.

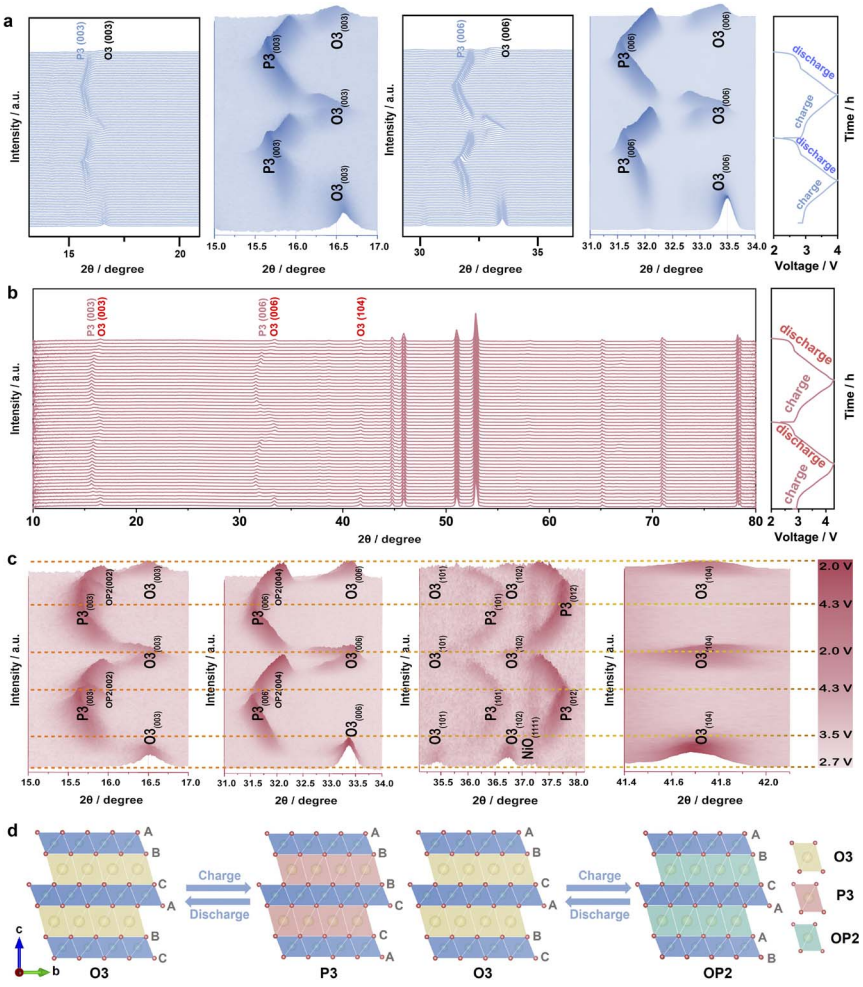

Fig. 4 Phase transition analysis of the NaNCMMT electrode during cycling. (a) *In situ* XRD patterns and 3D contour plots of characteristic peaks during the first two charge/discharge cycles at 0.1C in 2.0–4.0 V. (b) *In situ* XRD patterns for the first two charge/discharge cycles at 0.1C in 2.0–4.3 V. (c) 3D contour plots of diffraction peaks at 0.1C in 2.0–4.3 V. (d) Schematic illustration of structural changes during Na^+ extraction/insertion in 2.0–4.3 V.

Additionally, at 0.2C, the material maintains 75.3% of its capacity after 100 cycles, demonstrating excellent stability. Post-cycling SEM images reveal that the electrode morphology remains consistent with that of the pristine state, without any visible cracks (Fig. S10a–c, ESI†). Elemental distribution analysis using energy dispersive spectroscopy (EDS) confirms the uniform dispersion of Na, Ni, Cu, Mg, Mn, Ti, and O within the material (Fig. S10d, ESI†). These findings highlight the robustness of lattice oxygen in the NaNCMMT cathode under high-voltage conditions, providing valuable insights into its electrochemical stability and long-term durability.[56]

In situ XRD analyses were employed to investigate the crystal structure evolution of the NaNCMMT electrode during cycling in the voltage window of 2.0–4.0 V (Fig. 4a).[57–60] The results revealed a distinct phase-change process, which was captured through 3D contour graphs and intensity contour maps (Fig. S11a and S12a, ESI†). As Na^+ ions were extracted from the electrode, the (003) peak of the P3 phase appeared, signaling the transition from the O3 phase to the P3 phase.[61] Concurrently, a clear reduction in the (104) peaks associated with the O3 phase was observed, indicating a phase transition from O3 to P3. During Na^+ re-intercalation, the diffraction peaks reversed their trends, aligning well with the observed charge–discharge profiles. Notably, the second cycle mirrored the phase behavior of the initial one, affirming the reversibility of the O3 → P3 phase transition.[62,63] The voltage window was extended to 2.0–4.3 V to examine structural stability under more extreme conditions (Fig. 4b, c; and S11b, S12b, ESI†). Remarkably, the phase transition behavior observed in the 2.0–4.3 V range differed from that in the 2.0–4.0 V range due to the emergence of the OP2 phase. This phase, characterized by distinctive diffraction peaks associated with a mixed O–P stacking structure, became evident as Na^+ extraction progressed further. The extended voltage window triggered this additional transition, underscoring the electrode's capacity to accommodate significant structural changes. This reliable behavior suggests that Cu, Mg, and Ti co-substitution induces a fully reversible phase transition (O3 → P3 → OP2), as depicted more clearly in the crystal structure change diagram during cycling in 2.0–4.3 V (Fig. 4d). The incorporation of these co-substituent elements effectively stabilizes the crystal structure, enhancing the electrode's electrochemical performance by mitigating phase instability and reducing irreversible transitions.

High-temperature testing is crucial for evaluating the practical performance and stability of the NaNCMMT cathode.[64,65] The electrochemical properties of the sodium half-cell were assessed at 55 °C, a temperature known to induce structural changes in layered oxide cathodes, such as lattice destabilization and accelerated phase transitions, which can significantly affect the electrochemical stability. The analysis focused on two voltage ranges, 2.0–4.0 V and 2.0–4.3 V, providing a comprehensive assessment of the material's performance under high-temperature conditions. These conditions were selected to explore the material's behavior under realistic, thermally elevated scenarios, providing insights into its potential for high-temperature applications.[66] The rate performance data (Fig. 5a

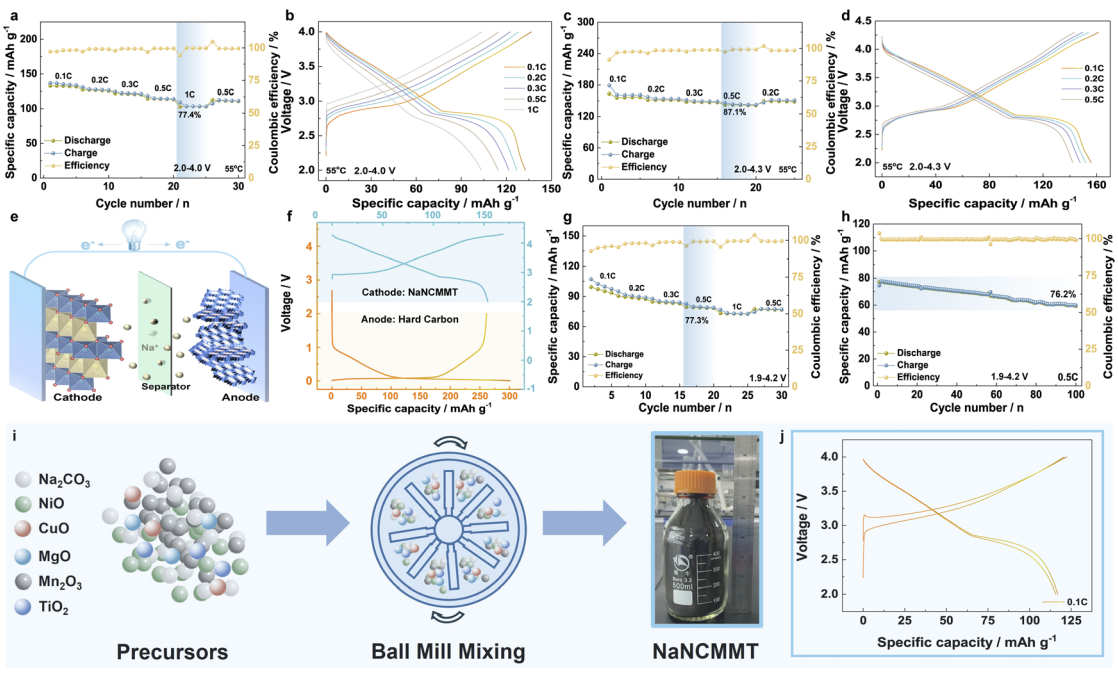

Fig. 5 High-temperature (55 °C) electrochemical performance of the NaNCMMT electrode. (a and b) Rate performance at various rates and the corresponding galvanostatic charge/discharge curves in 2.0–4.0 V. (c and d) Rate performance at various rates and the corresponding galvanostatic charge/discharge curves in 2.0–4.3 V. Electrochemical properties of a full battery system (NaNCMMT as cathode and hard carbon as anode). (e) Diagram illustrating the charging and discharging process. (f) Galvanostatic charge/discharge curves *versus* specific capacity of NaNCMMT cathode and hard carbon anode. (g) Rate performance at various rates. (h) Cycle performance during 100 cycles at 0.5C in 1.9–4.2 V. (i) The production process of industrial-grade NaNCMMT. (j) Galvanostatic charge/discharge curves of industrial-grade NaNCMMT at 0.1C in 2.0–4.0 V.

and b) revealed that, at 2.0–4.0 V, the NaNCMMT electrode retained 77.4% of its capacity when cycled at 1C compared to 0.1C. The NaNCMMT cathode exhibited a high reversible capacity of 132.8 mA h g^{-1} at 0.1C, which was notably greater than the capacity measured at room temperature. This enhancement in capacity under elevated temperature conditions is attributed to improved electrochemical reaction kinetics at the electrode–electrolyte interface.[67] Specifically, the increase in temperature accelerates charge and discharge processes, facilitating faster ion transport and more efficient electrochemical activity. Despite these gains, the cycling stability remained satisfactory, with a 73.9% retention rate after 100 cycles at 0.5C (Fig. S13a and b, ESI†). Expanding the voltage window to 2.0–4.3 V further demonstrated the material's steady performance. At 0.5C, the NaNCMMT electrode displayed an impressive 87.1% capacity retention compared to that at 0.1C, with cycle retention reaching 74.8% after 50 cycles at 0.2C (Fig. 5c and d; S13c, ESI†). The high-temperature testing confirmed that the Cu, Mg, and Ti co-doped NaNCMMT cathode maintains excellent electrochemical performance even under extreme conditions possibly due to the suppression of the Jahn–Teller effect by Ti substitution, thereby mitigating Mn dissolution. To investigate the cathode's practical application potential, a full cell was constructed pairing NaNCMMT as the cathode with hard carbon (HC) as the anode.[68] Fig. 5e illustrates schematically the operation of the full battery, and Fig. 5f presents the independent voltage distributions of the HC anode and NaNCMMT cathode in half-cells. Without pre-sodiation of the anode, the cell exhibited a specific capacity of 77.91 mA h g^{-1} within the 1.9–3.9 V range at 0.1C, maintaining 80.1% of its capacity at 0.5C compared to that at 0.1C (Fig. S14a and b, ESI†). Even after 100 cycles at 0.5C, the capacity retention was 77.6% (Fig. S14c, ESI†). Extending the voltage window to 1.9–4.2 V improved capacity to 102.72 mA h g^{-1}, with a retention rate of 77.3% at 0.5C compared to that at 0.1C and 76.2% after 100 cycles (Fig. 5g and h; S14d, ESI†). To further validate the practicality of the NaNCMMT cathode, the production process for industrial-grade NaNCMMT was examined (Fig. 5i; S15, ESI†).[69–71] Key characterizations reveal that the industrial-grade NaNCMMT exhibits a particle size distribution centered around 6.75 μm (Fig. S16a, ESI†), and shows uniform elemental distribution of Na, Ni, Cu, Mg, Mn, Ti, and O as confirmed by EDS mapping (Fig. S16b, ESI†). Although the electrochemical performance of the industrial-grade NaNCMMT is slightly reduced compared to lab-scale samples, it retains significant application potential. Performance could be further improved through optimizations like electrolyte adjustments or surface modifications (Fig. 5j; and S17, ESI†).

Conclusions

In summary, the Cu–Mg–Ti co-substitution strategy, guided by the principles of the periodic law, significantly improves the stability and electrochemical performance of O3-$NaNi_{0.5}Mn_{0.5}O_2$ cathodes, addressing key challenges such as structural instability, moisture sensitivity, and high-temperature degradation. The optimized material, O3-$NaNi_{0.4}Cu_{0.05}Mg_{0.05}Mn_{0.3}Ti_{0.2}O_2$, benefits from the synergistic effects of substituting Cu and Mg for Ni and Ti for Mn. Substituting Ni sites with Cu and Mg helps suppress irreversible phase transitions and enhance structural stability. Meanwhile, Mn site replacement with Ti not only enhances the material's high-voltage stability but also stabilizes the lattice oxygen (Scheme 1). These improvements in structure contribute to the material's excellent electrochemical performance: after 1000 cycles at 5C within the 2–4 V window, it retains 85% of its capacity, with fully reversible phase transitions. Additionally, the material is also highly resistant to moisture, maintaining a stable structure even in humid conditions. Moreover, it exhibits outstanding high-voltage stability. During charge–discharge cycling at a terminal voltage of 4.5 V, no oxygen release was observed, nor were any cracks detected in its morphology. Furthermore, the cathode exhibits excellent high-temperature stability in a half-cell and shows promising performance in a full cell, even without pre-sodiation. These findings illustrate the effectiveness of a periodic law-guided co-substitution approach in improving both stability and performance for sodium-ion cathodes, thereby offering valuable insights on how to design materials that will satisfy the demanding conditions typically experienced by systems for practical energy storage.

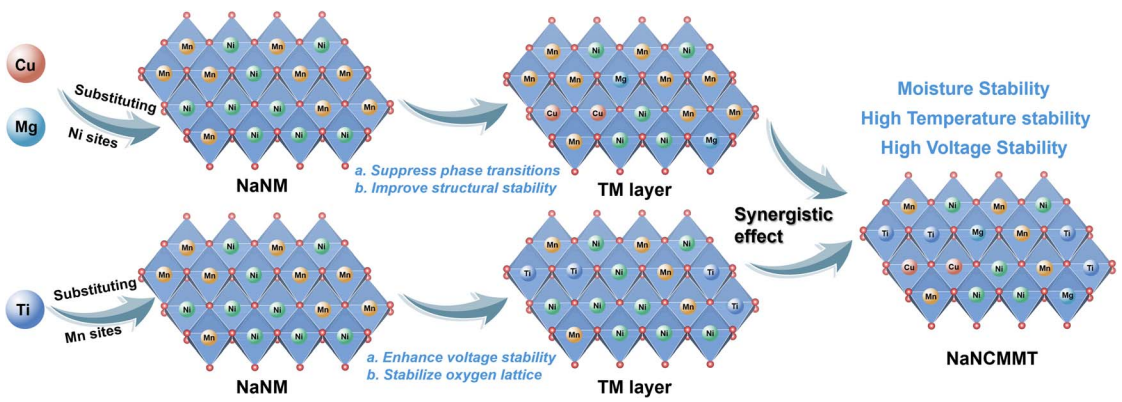

Scheme 1 Synergistic effects of Cu/Mg substitution for Ni and Ti substitution for Mn in NaNCMMT cathode.

Data availability

Essential data are fully provided in the main text and ESI.†

Author contributions

Yuan-Bo Wu: conceptualization, data curation, writing-original draft. Hai-Yan Hu: conceptualization, methodology, data analysis, manuscript revision. Jia-Yang Li: software, data curation. Hang-Hang Dong: methodology, data curation. Yan-Fang Zhu: project administration. Shuang-Qiang Chen: technical support. Na-Na Wang, Jia-Zhao Wang: resources. Yao Xiao: supervision, funding acquisition.

Conflicts of interest

There are no conflicts to declare.

Acknowledgements

This work was financially supported by the National Key R&D Program of China (2024YFA1211900), the National Natural Science Foundation of China (52402301, 52472240, 52202284), the Natural Science Foundation of Zhejiang Province (LQ23E020002), the Wenzhou Key Scientific and Technological Innovation Research Project (ZG2023053), the China Scholarship Council (202106370062), the Doctoral Innovation Foundation of Wenzhou University (3162023001001), and the Australia Research Council (DP240102926, FT240100596).

References

1 C. Vaalma, D. Buchholz, M. Weil and S. Passerini, *Nat. Rev. Mater.*, 2018, **3**, 18013.
2 J. Wang, Y. F. Zhu, Y. Su, J. X. Guo, S. Chen, H. K. Liu, S. X. Dou, S. L. Chou and Y. Xiao, *Chem. Soc. Rev.*, 2024, **53**, 4230–4301.
3 D. Eum, B. Kim, J.-H. Song, H. Park, H.-Y. Jang, S. J. Kim, S.-P. Cho, M. H. Lee, J. H. Heo, J. Park, Y. Ko, S. K. Park, J. Kim, K. Oh, D.-H. Kim, S. J. Kang and K. Kang, *Nat. Mater.*, 2022, **21**, 664–672.
4 Y. Su, B. Johannessen, S. Zhang, Z. Chen, Q. Gu, G. Li, H. Yan, J. Y. Li, H. Y. Hu, Y. F. Zhu, S. Xu, H. Liu, S. Dou and Y. Xiao, *Adv. Mater.*, 2023, **35**, e2305149.
5 H. Fu, Y.-P. Wang, G. Fan, S. Guo, X. Xie, X. Cao, B. Lu, M. Long, J. Zhou and S. Liang, *Chem. Sci.*, 2022, **13**, 726–736.
6 X. Wang, Q. Zhang, C. Zhao, H. Li, B. Zhang, G. Zeng, Y. Tang, Z. Huang, I. Hwang, H. Zhang, S. Zhou, Y. Qiu, Y. Xiao, J. Cabana, C.-J. Sun, K. Amine, Y. Sun, Q. Wang, G.-L. Xu, L. Gu, Y. Qiao and S.-G. Sun, *Nat. Energy*, 2024, **9**, 184–196.
7 Y. Tang, Q. Zhang, W. Zuo, S. Zhou, G. Zeng, B. Zhang, H. Zhang, Z. Huang, L. Zheng, J. Xu, W. Yin, Y. Qiu, Y. Xiao, Q. Zhang, T. Zhao, H.-G. Liao, I. Hwang, C.-J. Sun, K. Amine, Q. Wang, Y. Sun, G.-L. Xu, L. Gu, Y. Qiao and S.-G. Sun, *Nat. Sustain.*, 2024, **7**, 348–359.
8 J. Y. Li, H. Y. Hu, L. F. Zhou, H. W. Li, Y. J. Lei, W. H. Lai, Y. M. Fan, Y. F. Zhu, G. Peleckis, S. Q. Chen, W. K. Pang, J. Peng, J. Z. Wang, S. X. Dou, S. L. Chou and Y. Xiao, *Adv. Funct. Mater.*, 2023, **33**, 2213215.
9 Y. J. Guo, R. X. Jin, M. Fan, W. P. Wang, S. Xin, L. J. Wan and Y. G. Guo, *Chem. Soc. Rev.*, 2024, **53**, 7828–7874.
10 G. T. Park, N. Y. Park, H. H. Ryu, H. H. Sun, J. Y. Hwang and Y. K. Sun, *Chem. Soc. Rev.*, 2024, DOI: 10.1039/d3cs01110k.
11 Q. Wang, D. Zhou, C. Zhao, J. Wang, H. Guo, L. Wang, Z. Yao, D. Wong, G. Schuck, X. Bai, J. Lu and M. Wagemaker, *Nat. Sustain.*, 2024, **7**, 338–347.
12 H. Y. Hu, H. Wang, Y. F. Zhu, J. Y. Li, Y. Liu, J. Wang, H. X. Liu, X. B. Jia, H. Li, Y. Su, Y. Gao, S. Chen, X. Wu, S. X. Dou, S. Chou and Y. Xiao, *ACS Nano*, 2023, **17**, 15871–15882.
13 Y. Yu, Q. Mao, D. Wong, R. Gao, L. Zheng, W. Yang, J. Yang, N. Zhang, Z. Li, C. Schulz and X. Liu, *J. Am. Chem. Soc.*, 2024, **146**, 22220–22235.
14 D. Yang, X. W. Gao, G. Gao, Q. Lai, T. Ren, Q. Gu, Z. Liu and W. B. Luo, *Carbon Energy*, 2024, **6**, e574.
15 L. Qiu, M. Zhang, Y. Song, Z. Wu, Y. F. Zhu, J. Zhang, D. Wang, H. Y. Hu, H. W. Li, H. R. Liu, X. B. Jia, J. Peng, S. Chen, Z. Yang, Y. Xiao and X. Guo, *Carbon Energy*, 2022, **5**, e298.
16 S. Gao, Z. Zhu, H. Fang, K. Feng, J. Zhong, M. Hou, Y. Guo, F. Li, W. Zhang, Z. Ma and F. Li, *Adv. Mater.*, 2024, **36**, e2311523.
17 Y.-F. Liu, H.-Y. Hu, J.-Y. Li, H. Wang, Y. Zhao, J. Wang, Y.-B. Wu, Y.-J. Li, G.-Y. Zhang, Q.-Q. Sun, Y.-F. Zhu, R.-R. Tang, X.-W. Wu, J.-Z. Wang, S.-X. Dou, S.-L. Chou and Y. Xiao, *Sci. China:Chem.*, 2024, **67**, 4242–4250.
18 J. Li, H. Hu, J. Wang and Y. Xiao, *Carbon Neutralization*, 2022, **1**, 96–116.
19 Z. Li, H. Yi, H. Ren, J. Fang, Y. Du, W. Zhao, H. Chen, Q. Zhao and F. Pan, *Adv. Funct. Mater.*, 2023, **33**, 2307913.
20 Y. Xiao, H. R. Wang, H. Y. Hu, Y. F. Zhu, S. Li, J. Y. Li, X. W. Wu and S. L. Chou, *Adv. Mater.*, 2022, **34**, e2202695.
21 Z. Xu, K. Song, X. Chang, L. Li, W. Zhang, Y. Xue, J. Zhang, D. Lin, Z. Liu, Q. Wang, Y. Yu and C. Yang, *Carbon Neutralization*, 2024, **3**, 832–856.
22 S. He, X. Shen, M. Han, Y. Liao, L. Xu, N. Yang, Y. Guo, B. Li, J. Shen, C. Zha, Y. Li, M. Wang, L. Wang, Y. Su and F. Wu, *ACS Nano*, 2024, **18**, 11375–11388.
23 Y. F. Liu, K. Han, D. N. Peng, L. Y. Kong, Y. Su, H. W. Li, H. Y. Hu, J. Y. Li, H. R. Wang, Z. Q. Fu, Q. Ma, Y. F. Zhu, R. R. Tang, S. L. Chou, Y. Xiao and X. W. Wu, *InfoMat*, 2023, **5**, e12422.
24 H. Dong, H. Liu, Y. J. Guo, Y. H. Feng, X. Zhu, S. W. Xu, F. Sui, L. Yu, M. Liu, J. Z. Guo, Y. X. Yin, B. Xiao, X. L. Wu, Y. G. Guo and P. F. Wang, *J. Am. Chem. Soc.*, 2024, **146**, 22335–22347.
25 X.-Y. Zhang, H.-Y. Hu, X.-Y. Liu, J. Wang, Y.-F. Liu, Y.-F. Zhu, L.-Y. Kong, Z.-C. Jian, S.-L. Chou and Y. Xiao, *Nano Energy*, 2024, **128**, 109905.
26 C. Zhao, Q. Wang, Z. Yao, J. Wang, B. Sanchez-Lengeling, F. Ding, X. Qi, Y. Lu, X. Bai, B. Li, H. Li, A. Aspuru-Guzik,

X. Huang, C. Delmas, M. Wagemaker, L. Chen and Y.-S. Hu, *Science*, 2020, **370**, 708.
27 P. F. Wang, H. R. Yao, X. Y. Liu, J. N. Zhang, L. Gu, X. Q. Yu, Y. X. Yin and Y. G. Guo, *Adv. Mater.*, 2017, **29**, 1700210.
28 H. R. Yao, P. F. Wang, Y. Gong, J. Zhang, X. Yu, L. Gu, C. OuYang, Y. X. Yin, E. Hu, X. Q. Yang, E. Stavitski, Y. G. Guo and L. J. Wan, *J. Am. Chem. Soc.*, 2017, **139**, 8440–8443.
29 D. A. Edelman, D. Eum and W. C. Chueh, *Nat. Sustain.*, 2024, **7**, 234–235.
30 Y. Huang, Q. Zhang, X. G. Sun, K. Liu, W. Sun, M. Zhi, Y. Guo, S. Zheng and S. Dai, *Angew. Chem., Int. Ed.*, 2024, **136**, e202406277.
31 H. Wang, K. Lai, F. Guo, B. Long, X. Zeng, Z. Fu, X. Wu, Y. Xiao, S. Dou and J. Dai, *Carbon Neutralization*, 2022, **1**, 59–67.
32 L.-Y. Kong, J.-Y. Li, H.-X. Liu, Y.-F. Zhu, J. Wang, Y. Liu, X.-Y. Zhang, H.-Y. Hu, H. Dong, Z.-C. Jian, C. Cheng, S. Chen, L. Zhang, J.-Z. Wang, S. Chou and Y. Xiao, *J. Am. Chem. Soc.*, 2024, **146**, 32317–32332.
33 S. Huang, Y. Sun, T. Yuan, H. Che, Q. Zheng, Y. Zhang, P. Li, J. Qiu, Y. Pang, J. Yang, Z. F. Ma and S. Zheng, *Carbon Neutralization*, 2024, **3**, 584–596.
34 T. Zhang, M. Ren, Y. Huang, F. Li, W. Hua, S. Indris and F. Li, *Angew. Chem., Int. Ed.*, 2024, **63**, e202316949.
35 X. B. Jia, J. Wang, Y. F. Liu, Y. F. Zhu, J. Y. Li, Y. J. Li, S. L. Chou and Y. Xiao, *Adv. Mater.*, 2024, **36**, e2307938.
36 K. Momma and F. Izumi, *J. Appl. Crystallogr.*, 2011, **44**, 1272–1276.
37 T. Yuan, S. Li, Y. Sun, J. H. Wang, A. J. Chen, Q. Zheng, Y. Zhang, L. Chen, G. Nam, H. Che, J. Yang, S. Zheng, Z. F. Ma and M. Liu, *ACS Nano*, 2022, **16**, 18058–18070.
38 H. Y. Hu, J. Y. Li, Y. F. Liu, Y. F. Zhu, H. W. Li, X. B. Jia, Z. C. Jian, H. X. Liu, L. Y. Kong, Z. Q. Li, H. H. Dong, M. K. Zhang, L. Qiu, J. Q. Wang, S. Q. Chen, X. W. Wu, X. D. Guo and Y. Xiao, *Chem. Sci.*, 2024, **15**, 5192–5200.
39 L. Yu, X. He, B. Peng, F. Wang, N. Ahmad, Y. Shen, X. Ma, Z. Tao, J. Liang, Z. Jiang, Z. Diao, B. He, Y. Xie, B. Qing, C. Wang, Y. Wang and G. Zhang, *Adv. Funct. Mater.*, 2024, **34**, 2406771.
40 P. Masset and R. A. Guidotti, *J. Power Sources*, 2007, **164**, 397–414.
41 Z.-C. Jian, Y.-F. Liu, Y.-F. Zhu, J.-Y. Li, H.-Y. Hu, J. Wang, L.-Y. Kong, X.-B. Jia, H.-X. Liu, J.-X. Guo, M.-Y. Li, Y.-S. Xu, J.-F. Mao, S.-L. Zhang, Y. Su, S.-X. Dou, S.-L. Chou and Y. Xiao, *Nano Energy*, 2024, **125**, 109528.
42 S. Jia, S. Kumakura and E. McCalla, *Energy Environ. Sci.*, 2024, **17**, 4343–4389.
43 S. Guo, Q. Li, P. Liu, M. Chen and H. Zhou, *Nat. Commun.*, 2017, **8**, 135.
44 A. P. L. Oleksandr Bondarchuk, A. Kvasha, T. Thieu, E. Ayerbe and I. Urdampilleta, *Appl. Surf. Sci.*, 2021, **535**, 147699.
45 Y. G. Zou, H. Mao, X. H. Meng, Y. H. Du, H. Sheng, X. Yu, J. L. Shi and Y. G. Guo, *Angew. Chem., Int. Ed.*, 2021, **60**, 26535–26539.
46 C. Jiang, Y. Wang, Y. Xin, X. Ding, S. Liu, Y. Pang, B. Chen, Y. Wang, L. Liu, F. Wu and H. Gao, *Carbon Neutralization*, 2024, **3**, 233–244.
47 J. Y. Li, H. Y. Hu, H. W. Li, Y. F. Liu, Y. Su, X. B. Jia, L. F. Zhao, Y. M. Fan, Q. F. Gu, H. Zhang, W. K. Pang, Y. F. Zhu, J. Z. Wang, S. X. Dou, S. L. Chou and Y. Xiao, *ACS Nano*, 2024, **18**, 12945–12956.
48 X. Z. Wang, Y. Zuo, Y. Qin, X. Zhu, S. W. Xu, Y. J. Guo, T. Yan, L. Zhang, Z. Gao, L. Yu, M. Liu, Y. X. Yin, Y. Cheng, P. F. Wang and Y. G. Guo, *Adv. Mater.*, 2024, **36**, e2312300.
49 Y. F. Liu, H. Y. Hu, Y. F. Zhu, D. N. Peng, J. Y. Li, Y. J. Li, Y. Su, R. R. Tang, S. L. Chou and Y. Xiao, *Chem. Commun.*, 2024, **60**, 6496–6499.
50 Y. Xiao, Y. F. Liu, H. W. Li, J. Y. Li, J. Q. Wang, H. Y. Hu, Y. Su, Z. C. Jian, H. R. Yao, S. Q. Chen, X. X. Zeng, X. W. Wu, J. Z. Wang, Y. F. Zhu, S. X. Dou and S. L. Chou, *InfoMat*, 2023, **5**, e12475.
51 Y. Wang, J. Jin, X. Zhao, Q. Shen, X. Qu, L. Jiao and Y. Liu, *Angew. Chem., Int. Ed.*, 2024, **63**, e202409152.
52 Z. Chen, Y. Deng, J. Kong, W. Fu, C. Liu, T. Jin and L. Jiao, *Adv. Mater.*, 2024, **36**, e2402008.
53 T. Cui, L. Liu, Y. Xiang, C. Sheng, X. Li and Y. Fu, *J. Am. Chem. Soc.*, 2024, **146**, 13924–13933.
54 Y. J. Guo, P. F. Wang, Y. B. Niu, X. D. Zhang, Q. Li, X. Yu, M. Fan, W. P. Chen, Y. Yu, X. Liu, Q. Meng, S. Xin, Y. X. Yin and Y. G. Guo, *Nat. Commun.*, 2021, **12**, 5267.
55 S. Kim, H. S. Kim, B. Kim, Y. J. Kim, J. W. Jung and W. H. Ryu, *Adv. Energy Mater.*, 2023, **13**, 2301983.
56 Y.-F. Zhu, Y. Xiao, S.-X. Dou, Y.-M. Kang and S.-L. Chou, *eScience*, 2021, **1**, 13–27.
57 H. Y. Hu, Y. F. Zhu, Y. Xiao, S. Li, J. Y. Li, Z. Q. Hao, J. H. Zhao and S. L. Chou, *Adv. Energy Mater.*, 2022, **12**, 2201511.
58 W. Zhang, Y. Wu, Y. Dai, Z. Xu, L. He, Z. Li, S. Li, R. Chen, X. Gao, W. Zong, F. Guo, J. Zhu, H. Dong, J. Li, C. Ye, S. Li, F. Wu, Z. Zhang, G. He, Y. Lai and I. Parkin, *Chem. Sci.*, 2023, **14**, 8662–8671.
59 L.-Y. Kong, H.-X. Liu, Y.-F. Zhu, J.-Y. Li, Y. Su, H.-W. Li, H.-Y. Hu, Y.-F. Liu, M.-J. Yang, Z.-C. Jian, X.-B. Jia, S.-L. Chou and Y. Xiao, *Sci. China:Chem.*, 2023, **67**, 191–213.
60 M. Ren, S. Zhao, S. Gao, T. Zhang, M. Hou, W. Zhang, K. Feng, J. Zhong, W. Hua, S. Indris, K. Zhang, J. Chen and F. Li, *J. Am. Chem. Soc.*, 2023, **145**, 224–233.
61 Q. Wang, G. Yu, B. Luo, W. Ji, Z. Liu, M. Li, Y. Nong, Y. Tian, X. Wang, J. Zhang, C. L. Chen, C. K. Chang, Z. Sang, Z. Zhao, R. Zhao and J. Liang, *ACS Nano*, 2024, **18**, 18622–18634.
62 Y. Xiao, T. Wang, Y. F. Zhu, H. Y. Hu, S. J. Tan, S. Li, P. F. Wang, W. Zhang, Y. B. Niu, E. H. Wang, Y. J. Guo, X. Yang, L. Liu, Y. M. Liu, H. Li, X. D. Guo, Y. X. Yin and Y. G. Guo, *Research*, 2020, **2020**, 1469301.
63 C. Zheng, S. He, J. Gan, Z. Wu, L. She, Y. Gao, Y. Yang, J. Lou, Z. Ju and H. Pan, *Carbon Energy*, 2024, e605, DOI: **10.1002/cey2.605**.
64 Y. Zhu, W. Li, L. Zhang, W. Fang, Q. Ruan, J. Li, F. Zhang, H. Zhang, T. Quan and S. Zhang, *Energy Environ. Sci.*, 2023, **16**, 2825–2855.
65 F. Zhang, B. He, Y. Xin, T. Zhu, Y. Zhang, S. Wang, W. Li, Y. Yang and H. Tian, *Chem. Rev.*, 2024, **124**, 4778–4821.

66 Z. Cui and A. Manthiram, *Angew. Chem., Int. Ed.*, 2023, **62**, e202307243.
67 H. Liu, L. Kong, H. Wang, J. Li, J. Wang, Y. Zhu, H. Li, Z. Jian, X. Jia, Y. Su, S. Zhang, J. Mao, S. Chen, Y. Liu, S. Chou and Y. Xiao, *Adv. Mater.*, 2024, **36**, e2407994.
68 H.-Y. Hu, Y. Xiao, W. Ling, Y.-B. Wu, P. Wang, S.-J. Tan, Y.-S. Xu, Y.-J. Guo, W.-P. Chen, R.-R. Tang, X.-X. Zeng, Y.-X. Yin and X.-W. Wu, *Energy Technol.*, 2020, **9**, 2000730.
69 Y. Liao, L. Yuan, Y. Han, C. Liang, Z. Li, Z. Li, W. Luo, D. Wang and Y. Huang, *Adv. Mater.*, 2024, **36**, e2312287.
70 Z.-C. Jian, J.-X. Guo, Y.-F. Liu, Y.-F. Zhu, J. Wang and Y. Xiao, *Chem. Sci.*, 2024, **15**, 19698–19728.
71 B. Zhu, W. Zhang, Z. Jiang, J. Chen, Z. Li, J. Zheng, N. Wen, R. Chen, H. Yang, W. Zong, Y. Dai, C. Ye, Q. Zhang, T. Qiu, Y. Lai, J. Lia and Z. Zhang, *Chem. Sci.*, 2024, **15**, 14104–14121.